



Mechanistic investigation of the enhanced NH₃-SCR on cobalt-decorated Ce-Ti mixed oxide: *In situ* FTIR analysis for structure-activity correlation

Jie Liu ^{a,b}, Xinyong Li ^{b,*}, Qidong Zhao ^b, Jun Ke ^b, Huining Xiao ^a, Xiaojuan Lv ^a, Shaomin Liu ^c, Moses Tadé ^c, Shaobin Wang ^{c,*}

^a School of Environmental Science & Engineering, North China Electric Power University, Baoding, China

^b State Key Laboratory of Fine Chemicals, Key Laboratory of Industrial Ecology and Environmental Engineering (MOE), School of Environmental Science and Technology, Dalian University of Technology, Dalian, China

^c Department of Chemical Engineering, Curtin University, GPO Box U1987, Perth, WA 6845, Australia



ARTICLE INFO

Article history:

Received 27 April 2016

Received in revised form 22 June 2016

Accepted 15 July 2016

Available online 16 July 2016

Keywords:

Low-temperature NH₃-SCR

Nitrogen oxides (NO_x)

Surface Ce³⁺ species

In situ FTIR

Reaction mechanism

ABSTRACT

A series of transition metals (Co, Cu and Fe) were selected to decorate Ce-Ti mixed oxide to elevate the low-temperature activity of selective catalytic reduction of NO_x by NH₃ (NH₃-SCR) reaction, by adjusting the ratio of surface Ce³⁺ species and oxygen vacancies. Among them, Co-Ce-Ti sample exhibited the excellent low-temperature activity and broadened temperature window, which could be attributed to the improvement of the physico-chemical properties and the acceleration of the reactions in the Langmuir-Hinshelwood (L-H) and Eley-Rideal (E-R) mechanisms. Owing to the different ionic sizes of Co²⁺ and Ce⁴⁺, the lattice distortion of Ce-Ti mixed oxide was greatly aggravated and subsequently increased the ratio of Ce³⁺ and the surface adsorbed oxygen, which benefited the generation of adsorbed NO_x species and improved the reaction in the L-H mechanism. Meanwhile, the coordinatively unsaturated cationic sites over the Co-Ce-Ti sample induced more Lewis acid sites and enhanced the formation of the adsorbed NH₃ species bounded with Lewis acid sites, which were considered as the crucial intermediates in E-R mechanism, and therefore facilitating the reaction between the adsorbed NH₃ species and NO molecules. The enhancements in both the reactions from L-H and E-R mechanisms appeared to directly correlated with the improved deNO_x performance on the Co-Ce-Ti sample, and the L-H mechanism could be the dominate one at low temperatures due to its rapid reaction rate.

© 2016 Published by Elsevier B.V.

1. Introduction

The selective catalytic reduction (SCR) of NO_x with NH₃ is a well-established and efficient process for the elimination of NO_x emissions. As the most common commercial catalyst, V-W/Mo-TiO₂ exhibits good performance of deNO_x, but its high operation temperature window (300–400 °C), the toxicity of vanadium species, as well as the easy oxidation of SO₂ to SO₃ limit its further application [1–3]. Therefore, it is necessary to design new catalysts to tackle the above issues, especially the catalyst operation temperature (below 250 °C), which greatly helps resolve the issues of SO₂ oxidation and poisoning.

Owing to the shifting between Ce⁴⁺ and Ce³⁺ and the oxygen defects, CeO₂ has high reducibility and remarkable oxygen storage capacity (OSC), and therefore it is an appropriate candidate for the NH₃-SCR with low-temperature activity [4–7]. Up to date, some TiO₂-based materials modified by cerium have been reported as the SCR catalysts with high SO₂-resistance, and the Ce–O–Ti short-range order species with the interaction between Ce and Ti in atomic scale are proposed to be the active sites [8]. Whereas the temperature window of Ce-Ti mixed oxide catalysts is generally in 250–350 °C, exhibiting only a slight elevation of low-temperature activity compared with that of V-W/Mo-TiO₂ catalyst [9–11].

Besides CeO₂, transition metal oxides (such as CuO, Fe₂O₃, and Co₃O₄) have also attracted considerable attention due to their excellent redox property caused by the easy gain and lose of electrons in d shell of the metal cations, as well as their low price and high thermodynamic stability [12,13]. Transition metal oxides are widely reported as dopants to fabricate bi- or multi-metal

* Corresponding authors.

E-mail addresses: xinyongli@hotmail.com, xinyongli@hotmail.com (X. Li), shaobin.wang@curtin.edu.au (S. Wang).

oxides, and the resulted distortion of lattice structure, nontypical coordination modes and synergistic interactions of various compositions could be crucial for the improvement of the catalytic activity [14–16]. Meanwhile, the above changes often lead to the enhancement of the bonding strength of metal–oxygen and the increase of the formation of defects and oxygen vacancies, and therefore providing more active sites for the reactions [17–19]. Especially, for the Ce-containing materials used in SCR reaction, the doping of transition metal oxide benefits to increase the fraction of Ce³⁺ by establishing a close Ce–O–M (M = transition metal) interaction, which has a positive correlation with the quantity of oxygen vacancies [20,21], and the materials with abundant oxygen vacancies usually exhibit an improved capacity towards NO oxidation [19,22]. Moreover, according to recent reports [23–25], one of the transition metal-based materials, Co-based mixed oxide, have been considered as a promising candidate for low-temperature deNO_x catalysts, due to the readily formation of mixed bonds with strong interaction and the subsequent enhanced capacity of NO oxidation. Herein, the metal oxide materials containing the mixed bond of Ce–O–Co may be a novel low-temperature catalyst for NH₃-SCR reaction.

In the present study, we select some typical transition metals, M (M = Co, Cu and Fe) with variable valence to decorate the Ce–Ti mixed oxide, which were synthesized by a facile urea-homogeneous precipitation and a high dispersion of active species was obtained. The effect of M-doping on the ratio of surface Ce³⁺ species and the amount of vacancies, as well as the surface structure of materials were analyzed systematically by a series of physico-chemical characterizations (ICP, BET, XRD, EPR, XPS, H₂-TPR, TPD). *In-situ* FTIR spectroscopy was used to investigate the surface adsorbed species and the transformation of various intermediates, which greatly depends on the structure of catalysts and the property of dopant, and the mechanism for the enhancement of the low-temperature activity of catalyst is proposed. The findings in this work would contribute to the rational design of Ce-containing materials for NH₃-SCR by fine-tuning of the surface structure.

2. Experimental

2.1. Catalyst preparation

Ce–Ti, M–Ti and M–Ce–Ti (M = Co, Cu, Fe) mixed oxide catalysts were synthesized by a urea precipitation method. For the preparation of Ce–Ti catalyst, 0.375 mol of cerium ammonium nitrate ((NH₄)₂Ce(NO₃)₆) and titanium oxysulfate (TiOSO₄·H₂O), with the Ce/Ti molar ratio of 0.1/0.9, and 35 g of urea (CO(NH₂)₂) were dissolved in deionized water of 500 mL. The above mixed solution was stirred at 90 °C for 8 h, and the obtained slurry was filtered, washed, dried and calcined at 400 °C for 4 h, with a heating rate of 10 °C min⁻¹. The synthesis of M–Ce–Ti was similar to that of Ce–Ti, in which partial (NH₄)₂Ce(NO₃)₆ was replaced by cobalt nitrate (Co(NO₃)₂·6H₂O), copper nitrate (Cu(NO₃)₂·3H₂O) or ferric nitrate (Fe(NO₃)₃·9H₂O), and the molar ratio of M/Ce/Ti was 0.05/0.05/0.9, with the sum of the molar ratios of metal elements of 1.0. For the M–Ti samples, the molar ratio of M/Ti was 0.05/0.9, with the sum of the molar ratios of metal elements of 0.95.

2.2. Catalyst characterization

The Brunauer–Emmett–Teller (BET) surface areas of the catalysts were measured by physical adsorption of N₂ at –196 °C using Micromeritics ASAP 2020. The sample was degassed at 300 °C for 4 h under vacuum prior to the BET determination.

Inductively coupled plasma-optical emission spectrometry (ICP-OES) was performed on a Leeman Profile spec apparatus to

determine the actual concentrations of various elements in catalysts.

Powder X-ray diffraction (XRD) was performed on a Rigaku D/Max 2550VB/PC X-ray powder diffractometer (XRD) using a Cu K α radiation ($\lambda = 0.154056$ nm), with a scanning rate of 10° min⁻¹.

Electron paramagnetic resonance (EPR) analysis was performed on Bruker (A200-9.5/12) at room temperature, operating at the X band (~9.8 GHz). The magnetic field was modulated at 100 kHz and the g value was determined from the precise frequency and magnetic field values.

X-ray photoelectron spectra (XPS) were recorded using a Thermo ESCALAB 250XI electron spectrometer. Binding energies of Ce 3d, Co 2p and O 1s were calibrated using C 1s (BE = 284.8 eV) as a standard.

Hydrogen-temperature programmed reduction (H₂-TPR) was carried out on Chembet PULSAR TPR/TPD (p/n 02139-1). The sample (50 mg) was pretreated at 400 °C for 1 h in He flow, followed by cooling to room temperature. The measurement range of H₂-TPR was 200–850 °C, in a stream of 10 vol.% H₂/Ar, with a heating rate of 10 °C min⁻¹.

Temperature-programmed desorption (TPD) was performed in a fixed-bed reactor with a computer-interfaced quadruple mass spectrometer (MS) as detector. For the NH₃-TPD, after the adsorption of NH₃ ([NH₃] = 500 ppm, with He as balance) at room temperature, the reactor was heat in the temperature range of 50–650 °C with a linear heating rate of 10 °C min⁻¹ in a flow of He, and the fragments of $m/z = 16$ was used to identify NH₃ in order to avoid the disturbance of $m/z = 17$ by H₂O. The NO-TPD was similar with that of NH₃-TPD, just changing the gas mixture to NO/O₂/He, in which the concentrations of NO and O₂ were 500 ppm and 5 vol.%, respectively, balanced with He, and the fragments of $m/z = 30$ was used to identify NO.

2.3. Catalytic tests

The SCR activity of various catalysts was measured in a fixed-bed reactor containing 200 mg catalyst (40–60 mesh). The typical reactant gas composition was as follows: [NO] = [NH₃] = 500 ppm, [O₂] = 5 vol.%, [SO₂] = 100 ppm (when used), with He as balance, and the hourly space velocity (GHSV) of approximately 30,000, 60,000 and 100,000 h⁻¹. The concentrations of NO in the inlet and outlet gases were measured using a chemiluminescence gas analyzer (Testo 350). The outlet gas N₂ was analyzed by an online gas chromatograph (Agilent 7890II) equipped with a 5A molecular sieve column. The NO_x conversion and N₂ selectivity were calculated accordingly.

To better evaluate the catalytic activity, the kinetic parameter was normalized on a per-sample weight basis, using NO_x conversion below 15% and calculated according to the following equation:

$$k = -\frac{V}{w} \times \ln(1 - x)$$

where k is the reaction rate constant (cm³ g⁻¹ g⁻¹), V is the total gas flow rate (cm³ s⁻¹), w is the mass of catalyst, and x is the NO conversion. The equation is based on the conditions that the reaction is first order dependence of NO and zero order dependence of NH₃ [26–28].

The oxidation of NO to NO₂ was measured in the same fixed-bed quartz reactor with 0.2 g catalyst, and the conditions were as follows: [NO] = 500 ppm, [O₂] = 5 vol.%, with He as balance, and the hourly space velocity (GHSV) of approximately 30,000 h⁻¹. The concentrations of NO and NO₂ in the inlet and outlet gases were measured using a chemiluminescence gas analyzer (Testo 350).

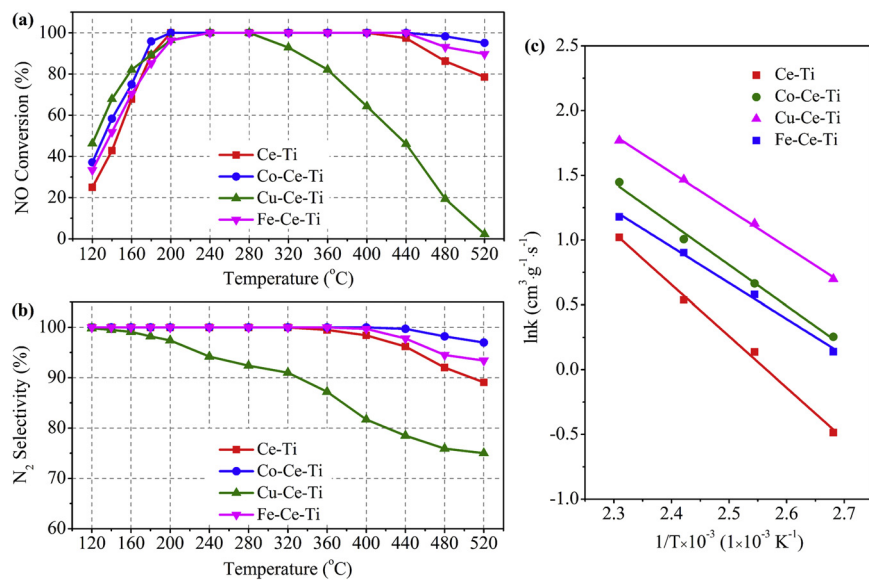


Fig. 1. NO conversions (a), N₂ selectivity (b), and the Arrhenius plot (c) of Ce-Ti and various M-Ce-Ti catalysts. Reaction conditions: [NO]=[NH₃]=500 ppm, [O₂]=5 vol.%, with He as balance.

2.4. In situ FT-IR study

In situ FT-IR spectra were recorded using a FTIR spectrometer (Bruker VERTEX 70-FTIR). Prior to each experiment, the sample (~20 mg) was pretreated in He stream (50 ml min⁻¹) at 400 °C for 1 h to remove the moisture, and then cooled to the desired temperature. All spectra were recorded over accumulative 32 scans with a resolution of 4 cm⁻¹ in the range of 4000–400 cm⁻¹. The concentrations of NO, NH₃, and O₂ in the gas mixture were 500 ppm, 500 ppm, and 5 vol.%(when used), respectively, with He as balance, and the flow rate of mixed gas was 50 ml min⁻¹.

3. Results and discussion

3.1. Catalytic test

3.1.1. NH₃-SCR activity under ideal conditions

Fig. 1a and b compares the NO conversion and N₂ selectivity of Ce-Ti and M-Ce-Ti mixed oxide catalysts depending on reaction temperatures, respectively. With the increase of reaction temperature, the NO conversion over Ce-Ti sample was elevated and achieved the maximum conversion of 100% at 200 °C, which maintained up to 420 °C. With the further increase of temperature, the SCR performance was inhibited slightly due to the enhancement of the direct oxidation of NH₃, and the NO conversion at 500 °C was decreased to 80.6%. To obtain a better SCR performance with good low-temperature activity and broadened temperature window, partial Ce atoms in Ce-Ti sample were substituted by Co, Cu, or Fe, and the catalytic activities of the M-Ce-Ti samples are also displayed in Fig. 1a. The substitution by Co or Cu generated the promotion of the low-temperature activity (120–180 °C), but the elevation did not occur over Fe-Ce-Ti sample. Whereas the Cu-Ce-Ti sample exhibited a quite narrow reaction temperature window, and the NO conversion dropped significantly from 300 °C and decreased further to 10.0% when the temperature increased to 500 °C. In contrast, the introduction of both Co and Fe increased the deNO_x activity at high temperatures and maintained the high activity (>90%) even at the temperature up to 500 °C. Fig. 1b suggested the enhanced N₂ selectivity caused by Co or Fe doping, while the N₂ selectivity of Cu-Ce-Ti sample was decreased compared with that of Ce-Ti sample.

The reaction rate constants (*k*) of the Ce-Ti and M-Ce-Ti samples have been calculated to better evaluate the catalytic activity, and the corresponding Arrhenius plots of the SCR reaction over these catalysts are presented in Fig. 1c. The absolute values of the slope of the fitting lines displayed the apparent activated barriers of the SCR reaction. The introduction of the transition metals decreased the energy barriers of reaction, and all the M-Ce-Ti samples exhibited a higher reaction rate than that of Ce-Ti.

The catalytic activities of M-Ti mixed oxide catalysts (M=Co, Cu, Fe) were also measured and the results are presented in Fig. S1 (Supporting information). The Cu-Ti sample exhibited a quite similar performance with that of Cu-Ce-Ti, an excellent low-temperature activity but a narrow reaction temperature window. For the Co-Ti and Fe-Ti samples, a poor low-temperature activity was observed with the NO conversions of less than 60% at 180 °C. Moreover, the reaction temperature window of Co-Ti sample at NO conversion (>80%) was only in the temperature range of 200–340 °C. Similarly, the activity of Fe-Ti sample at high temperatures was also declined compared with that of Fe-Ce-Ti sample.

The combining results in Figs. 1 and S1 suggested that Co could be the appropriate candidate to further optimize the catalytic performance of Ce-Ti sample. The synergistic effect of Co and Ce was speculated to benefit the decrease of the apparent activated barriers of SCR reaction, the increase of the reaction rate, and the consequent enhancement of the low-temperature activity and the broadening of reaction temperature window.

3.1.2. Effect of GHSV, H₂O and SO₂

Fig. 2a shows the effect of GHSV and the presence of H₂O on the NH₃-SCR performance of Co-Ce-Ti catalyst. Compared with the ideal reaction condition, the presence of H₂O led to a slight decrease of NO conversion under the GHSV of 30,000 h⁻¹ at low temperatures, while a similar activity at higher temperature (>200 °C) with that without H₂O. Furthermore, the increase of GHSV did not result in an obvious decrease of NO conversion over Co-Ce-Ti sample, suggesting that the novel Co-Ce-Ti catalyst is highly resistant to the large space velocity.

As the residual SO₂ in exhaust fumes may result in the poisoning and deactivation of catalyst, the stability of Ce-Ti and Co-Ce-Ti catalysts was measured at the co-existence of H₂O and SO₂ under different GHSV conditions at the low temperature of 180 °C. As dis-

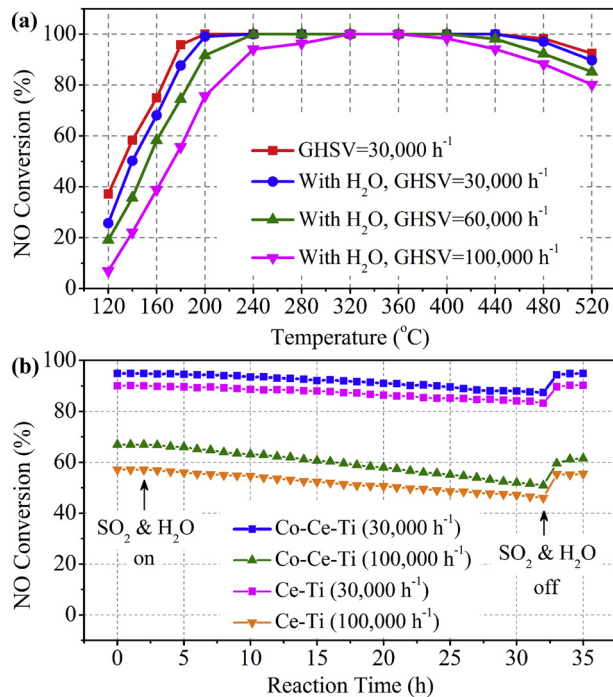


Fig. 2. (a) NH₃-SCR activity of Co-Ce-Ti catalyst under different GHSV in the presence of H₂O. (b) Comparison of the stability of Ce-Ti and Co-Ce-Ti samples in the co-existence of H₂O and SO₂ under different GHSV at 180 °C. Reaction conditions: [NO] = [NH₃] = 500 ppm, [O₂] = 5 vol.%, [H₂O] = 5 vol.%, [SO₂] = 100 ppm, with He as balance.

Table 1

Analysis of chemical compositions and physical properties of Ce-Ti, Co-Ti and Co-Ce-Ti samples.

Catalyst	Metal concentrations from ICP (wt.%)			Surface area (m ² g ⁻¹)
	Ce	Ti	Co	
Ce-Ti	9.69	34.14	–	153.7
Co-Ti	–	39.13	2.34	113.7
Co-Ce-Ti	5.08	38.05	1.82	191.1

played in Fig. 2b, the Co-Ce-Ti sample exhibited a satisfied stability in the presence of H₂O and SO₂, with the corresponding GHSV of 30,000 h⁻¹, which was similar with that of Ce-Ti. Under the higher GHSV of 100,000 h⁻¹, the Co-Ce-Ti sample also shown a higher NO conversion than that of Ce-Ti sample, though the poisoning caused by H₂O and SO₂ was slightly enhanced compared with that over Co-Ce-Ti sample. The results of the stability measurement suggested that the introduction of Co not only improved the low-temperature activity of SCR reaction, but also maintained the good capacity of catalyst resisting the poisoning of H₂O and SO₂.

3.2. Analysis of chemical compositions and physical properties

The chemical compositions and surface areas of Ce-Ti, Co-Ce-Ti and Co-Ti catalysts have been measured by ICP and N₂ adsorption-desorption, respectively, and the results are presented in Table 1. The concentrations of various metal elements were almost identical with the theoretical contents expressed by molar fractions (the information of Cu-Ce-Ti and Fe-Ce-Ti samples is shown in Table S1 in the Supporting information). The BET results illustrated that the surface area of Co-Ce-Ti sample was increased significantly compared with that of Ce-Ti and Co-Ti sample, which could be attributed to the structural distortion and disorder caused by the incorporation of Co. Similar phenomenon was also observed over Cu-Ce-Ti and Fe-Ce-Ti samples, the surface area of which was

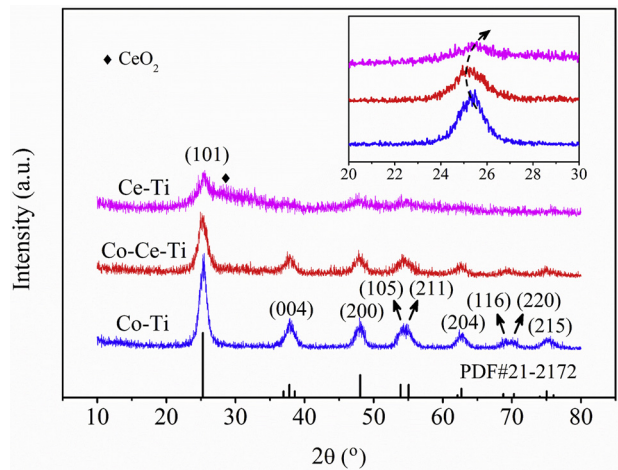


Fig. 3. XRD patterns of Co-Ti, Ce-Ti and Co-Ce-Ti samples (Insert: the enlarged XRD patterns of various samples in the 20 range of 20–30°).

enlarged compared with that of Ce-Ti sample (Table S1 in Supporting information). The increased surface area of M-Ce-Ti benefited the mass transfer and may also improve the adsorption and activation of reactants during the reaction.

The XRD patterns of Ce-Ti, Co-Ti and Co-Ce-Ti catalysts are shown in Fig. 3. The recorded peaks of Co-Ti samples were quite identical to the XRD patterns of tetragonal anatase TiO₂ (PDF#21-2172), indicating the formation of Co-Ti solid solution as well as the high dispersion of CoO_x in the bulk of TiO₂. The diffraction peaks over Co-Ce-Ti sample was similar with that of Co-Ti, though the intensity was weakened and the location of peak assigned to (101) plane shifted to the lower angles slightly. CoO_x and CeO₂ also existed as finely dispersed species, leading to the absence of corresponding characteristic peaks. By comparison, the diffraction peaks of Ce-Ti sample were broadened significantly and the corresponding intensities were also decreased. Besides, a shoulder peak appeared at 28.5° and was assigned to (111) phase of cubic CeO₂, which confirmed the formation of crystalline phase of CeO₂ as well as the lower dispersion of CeO₂ in Ce-Ti sample. The ionic sizes of Ti⁴⁺, Ce⁴⁺ and Co²⁺ are 0.64 Å, 0.97 Å and 0.58 Å, respectively. Due to the much larger size of Ce⁴⁺ than Ti⁴⁺, the Ce⁴⁺ could readily substitute to the Ti⁴⁺ sites, and the appearance of the diffraction peaks of CeO₂ over Ce-Ti sample could be attributed to the aggregation of CeO₂ caused by the excessive introduction of Ce⁴⁺. Whereas, Co²⁺ was speculated to mainly incorporate into the interstitial sites of lattice structure due to its smaller size, which could be further confirmed by ESR analysis later. Moreover, the XRD patterns of the fresh and used Co-Ce-Ti samples after the stability measurement were compared, as presented in Fig. S2 (Supporting information). The pattern of the used catalyst was quite similar with that of the fresh one, and there was no obvious characteristic peak of the separated CoO_x or CeO₂ particles, which could be an important reason for the well stability of Co-Ce-Ti sample.

3.3. ESR

ESR spectroscopy is a quite effective probe to elucidate the coordination geometry of transition metal ions as well as the valence states. The ESR experiment has been carried out for Co-Ti, Ce-Ti and Co-Ce-Ti catalysts at room temperature, and the results are depicted in Fig. 4. All of the three catalysts exhibited a sharply isotropic signal with *g* = 1.997. According to the report [29], this signal was ascribed as a type of Ti vacancies, which were produced by the doping of Ce and/or Co atoms and the further generation of O-rich environment between Ti-O-Ti parallel lattice chains. Com-

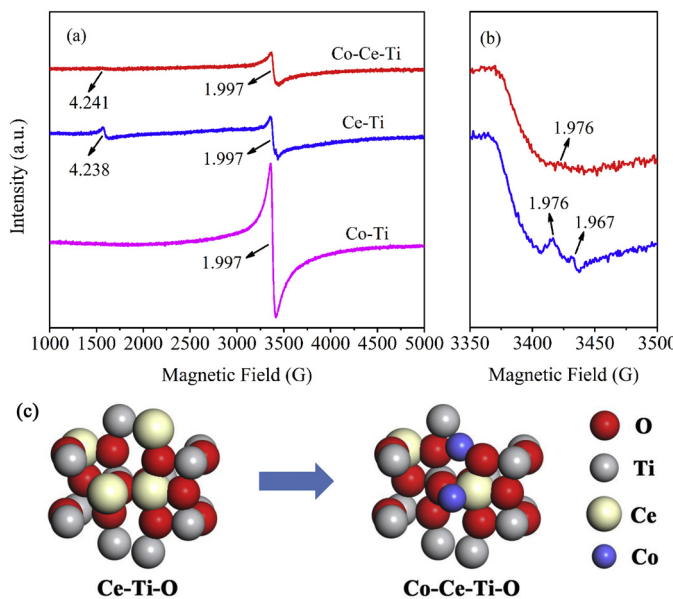


Fig. 4. (a) ESR spectra of Co-Ti, Ce-Ti and Co-Ce-Ti catalysts, (b) the magnified ESR spectra of Ce-Ti and Co-Ce-Ti catalysts in the range of 3350–3500G, and (c) the diagram of Co^{2+} incorporated in the interstitial sites of lattice structure.

pared with Ce-Ti and Co-Ce-Ti catalysts, Co-Ti sample exhibited a much stronger signal, illustrating the abundant lattice defects due to the unstoichiometric substitution of Ti atoms by Co atoms as well as the different charges of Co and Ti ions.

For the Ce-containing catalysts, some new signals appeared. The lines with g values of 4.241 and 4.238 from Co-Ce-Ti and Ce-Ti samples, respectively, suggesting the presence of Ce^{3+} ions with orthorhombic symmetry [30]. The weak signals with g values of 1.976 and 1.967, which were generally observed in Ce-containing materials, were assigned to the unpaired electrons trapped in defects or localized in anion vacancies coupled to Ce^{3+} ions [31–33]. Compared with Ce-Ti sample, the ESR spectra of Co-Ce-Ti sample exhibited the broadened linewidth and weakened intensity, illustrating the destroyed paramagnetic centers caused by the redistribution of Ce atoms. Moreover, due to the much smaller ionic size of Co^{2+} (0.58 Å) compared with Ce^{4+} (0.97 Å), the introduced Co^{2+} may substitute Ce^{4+} sites or incorporate into the interstitial sites of lattice structure. For the Ce^{4+} sites, oxygen vacancies are necessary for the charge balance, while for the interstitial sites, excess oxygen species are expected [34]. As the weak ESR signals generally suggest a high degree of lattice distortion [35], the Co^{2+} ions were considered to mainly occupy the interstitial sites, which could aggravate the lattice distortion by increasing the lattice constraint. Meanwhile, the diffusion of surface adsorbed oxygen associated with interstitial Co^{2+} to oxygen vacancies decreased the concentration of oxygen vacancies and lowered the ESR signals. The ESR spectra illustrated the high degree of coordinately unsaturated environment in Co-Ce-Ti sample, which was considered to greatly benefit the coupling of gas-phase NO molecules during NH_3 -SCR reaction.

3.4. X-ray photoelectron spectroscopy

XPS analysis has been performed to confirm the surface concentrations and chemical state of various elements over Ce-Ti, Co-Ti and Co-Ce-Ti samples. The results are summarized in Table 2, and the XPS spectra of Ce 3d, Co 2p and O 1s of various catalysts are displayed in Fig. 5. As presented in Fig. 5a, the XPS spectra in the Ce 3d region for Ce-Ti and Co-Ce-Ti samples were fitted into eight components in accordance with the report [36]. The peaks labeled as

Table 2

Surface atomic concentrations and relative concentration ratios of different species over Ce-Ti, Co-Ti and Co-Ce-Ti samples analyzed from XPS data.

Sample	Ce (%)	Ti (%)	Co (%)	O (%)	$\text{Ce}^{3+}/\text{Ce} (%)$	$\text{Co}^{3+}/\text{Co} (%)$	$\text{O}_\text{A}/\text{O} (%)$
Ce-Ti	2.4	29.7	–	67.9	41.1	–	18.3
Co-Ti	–	30.4	3.1	66.5	–	47.7	15.9
Co-Ce-Ti	1.2	30.9	0.7	67.2	45.2	50.5	24.1

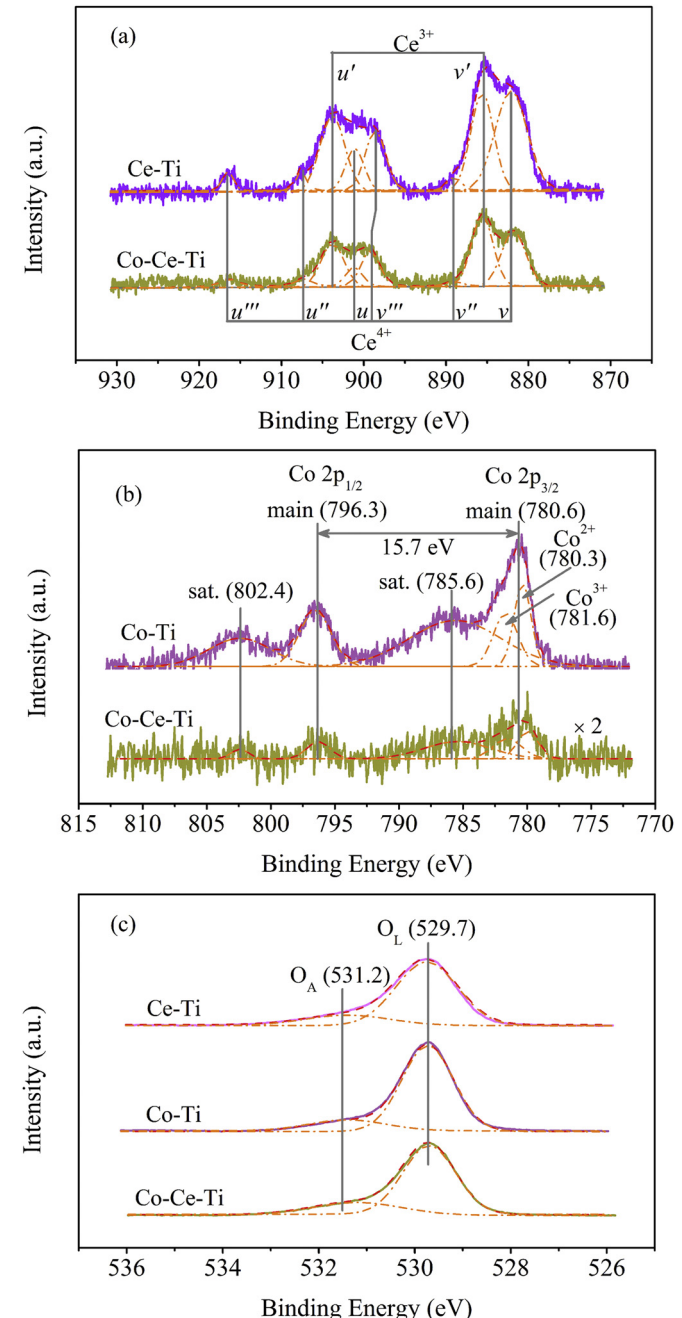


Fig. 5. XPS spectra for Ce 3d (a), Co 2p (b) and O 1s (c) of Ce-Ti, Co-Ti and Co-Ce-Ti samples.

u (901.1 eV), u'' (907.4 eV) and u'''' (916.6 eV) are arising from Ce^{4+} $3\text{d}_{3/2}$, and the bands labeled as v (882.1 eV), v'' (889.1 eV) and v'''' (898.6 eV) are arising from Ce^{4+} $3\text{d}_{5/2}$, while the presence of Ce^{3+} is confirmed by the peaks labeled as u' (903.8 eV) and v' (885.5 eV). The relative surface ratio of Ce^{3+} has been calculated by the corresponding peak areas to interpret the change of chemical state of Ce

caused by the partial substitution of Co. As presented in Table 2, the surface Ce³⁺ ratio over Co-Ce-Ti sample was 45.2%, slightly higher than that of Ce-Ti sample of 41.1%, illustrating the facilitated transformation of Ce⁴⁺ to Ce³⁺ caused by Co incorporation.

Fig. 5b shows the XPS spectra of Co 2p region for Co-Ti and Co-Ce-Ti samples. The Co 2p core level spectra in both the samples were characterized by two components resulting from spin-orbital splitting (Co 2p_{3/2} and Co 2p_{1/2}) and shake-up satellites, and the spin-orbital splitting between the Co 2p_{3/2} and Co 2p_{1/2} peaks of 15.7 eV, as well as the strong satellite peaks at higher BE, indicating the presence of Co²⁺ [37,38]. Moreover, the Co 2p_{3/2} peak could be fitted into two peaks assigned to Co²⁺ (780.3 eV) and Co³⁺ (781.6 eV), respectively, and the calculated relative surface contents of Co³⁺ on Co-Ti and Co-Ce-Ti samples were 47.7% and 50.5%, respectively, as presented in Table 2. Herein, it was inferred that the co-existence of Ce and Co benefited the transformation from Ce⁴⁺ to Ce³⁺ and Co²⁺ to Co³⁺. In general, a higher Ce³⁺ ratio indicates the presence of more surface oxygen vacancies generated by the charge compensation and means an easier adsorption of oxygen species and the easier activation of reductants. Meanwhile, the presence of more Co³⁺ species also benefits the acceleration of the chemisorption and activation of NH₃, which could be attributed to the enhancement of the redox properties of Co-based catalysts [39–41].

Fig. 5c compares the XPS spectra of O 1s of Ce-Ti, Co-Ti and Co-Ce-Ti catalysts, which have been fitted into two sub-bands and denoted as O_A (531.2 eV) and O_L (529.7 eV), respectively. The O_A peak corresponds to the surface adsorbed oxygen, such as O₂²⁻ or O⁻ belonging to a defect oxide, and the O_L peak is assigned to the lattice oxygen [42]. The relative molar ratios of O_A on various catalysts are displayed in Table 2, decreasing by the following order: Co-Ce-Ti (24.1%)>Ce-Ti (18.3%)>Co-Ti (15.9%). Due to the readily formation of oxygen vacancies caused by the presence of Ce³⁺, more oxygen species are readily to be adsorbed on catalyst surface, leading to the higher concentration of O_A species over Ce-Ti sample compared with that over Co-Ti sample. For Co-Ce-Ti sample, the introduced Co²⁺ ions benefited the adsorption of excess oxygen on the catalyst surface due to their occupation in the interstitial sites of lattice structure (analyzed in Section 3.3), leading to the further increase of the ratio of O_A species. Moreover, the surface defects, including charges imbalance and unsaturated chemical bonds, also facilitated the generation of defect oxygen and consequently elevated the O_A ratio. Compared with O_L species, the O_A species possessed the higher mobility and exhibited much higher activity in oxidation reactions. Herein, the catalyst with a higher ratio of O_A was speculated to benefit the oxidation of NO to NO₂, which was confirmed by the measurement of catalyst capacity towards NO oxidation, carried out over Ce-Ti, Co-Ti and Co-Ce-Ti samples (Fig. S3 in Supporting information). The easier oxidation of NO to NO₂ over Co-Ce-Ti sample also meant the accelerated transformation of NO₂ to nitrates, as well as the possible improvement of deNO_x performance via the enhanced “fast SCR” reaction.

3.5. H₂-TPR

The reducibility of catalysts has been measured by H₂-TPR, and the corresponding profiles are fitted into several peaks by Gaussian method based on the different reducibility of various species (Fig. 6). For Ce-Ti catalyst, there was only one broad peak around 554 °C (noted as γ), with a quite low intensity. As TiO₂ is difficult to be reduced, this peak was ascribed as the reduction of the surface-capping oxygen of CeO₂ [43,44]. For the Co-containing samples, the signals were mainly caused by the reduction of cobalt oxides. The α (504 °C) and β (584 °C) peaks over Co-Ti sample were attributed to the two-step reduction of cobalt oxides, Co³⁺→Co²⁺ and Co²⁺→Co⁰ [45–47]. By comparison, the reduction peaks of α

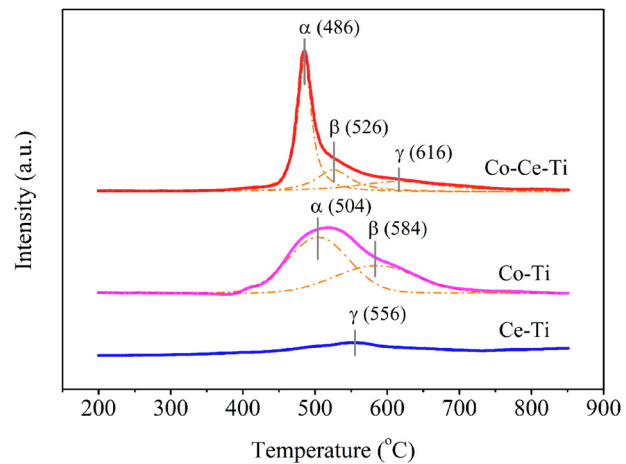


Fig. 6. H₂-TPR profiles of Ce-Ti, Co-Ti and Co-Ce-Ti samples.

and β over Co-Ce-Ti catalyst shifted to the lower temperature of 486 and 526 °C, respectively. The shift of the α and β peaks means the easier reduction of cobalt oxides, illustrating the weakened strength of Co–O–Co bonds caused by the strong interaction between the Co–O–Ce bond over Co-Ce-Ti sample. Besides, the peak at high temperature detected at 616 °C may also relate to the reduction of Co²⁺ bounded with ceria oxides, suggesting the formation of Co–O–Ce mixed bond though it may overlap with the reduction of surface oxygen over CeO₂ [45].

3.6. Adsorption and desorption properties

Adsorption of NO on the catalyst's surface has been reported to play an important role in the SCR reaction, herein, the NO-TPD experiment has been carried out on the Ce-Ti and Co-Ce-Ti samples and the results are displayed in Fig. 7a. For the Ce-Ti sample, the first peak located at about 80 °C was attributed to the physical desorption of NO_x, and the peaks at 100–200 °C was ascribed to the decomposition of chemical desorption of NO_x (ad-NO₂⁻). The peak at 200–300 °C was ascribed to the decomposition of monodentate nitrate [28,48]. For the Co-Ce-Ti sample, the peak area of the chemical desorption of NO_x was increased significantly, as shown in the inserted figure in Fig. 7a, while the quantity of the decomposed monodentate nitrate was similar with that on Ce-Ti sample. The NO-TPD results illustrated that the introduction of Co and the consequently formation of Co–O–Ce or Co–O–Ti mixed bonds increased the unstable surface NO_x species at low temperature.

As the chemisorption and activation of NH₃ was considered as the primary process in the NH₃-SCR reaction, the NH₃-TPD was also performed to investigate the quantity of the surface acids as well as the acid strength, and the results are presented in Fig. 7b. Both the samples displayed two broad NH₃ adsorption peaks, locating at the temperature range of 70–200 °C and 250–490 °C, assigned to the weakly adsorbed ammonia and the mid-strong acid sites, respectively [25,49]. By comparing the amount of NH₃ desorption, it was concluded that the introduction of Co played a positive effect on providing mid-strong acid sites. According to previous reports [24,28], the NH₃ molecules coordinated to the Lewis acid sites exhibit a higher thermal stability than that of the NH₄⁺ ions bound to the Brønsted acid sites, herein, the mid-strong acid sites could mainly be the Lewis acid sites. The NH₃-TPD results suggested the more Lewis acid sites over Co-Ce-Ti sample as well as the possible stronger capacity of Co-Ce-Ti sample towards NH₃ activation, which was further confirmed by the *in situ* FTIR spectra of NH₃ adsorption as follow.

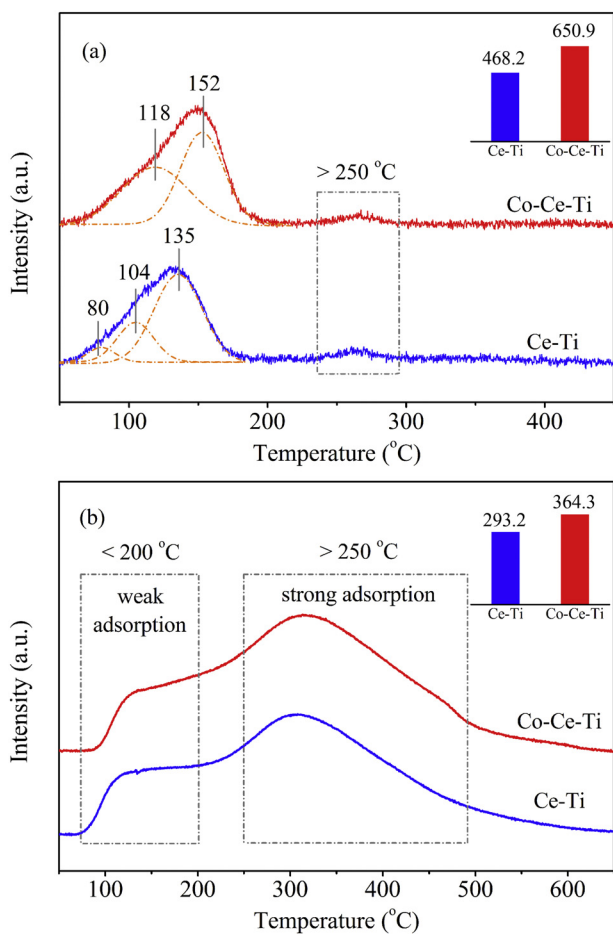


Fig. 7. NO-TPD (a) and NH₃-TPD (b) profiles of Ce-Ti and Co-Ce-Ti samples. (Insert: the integral area of NO_x and NH₃ from NO-TPD and NH₃-TPD profiles).

3.7. In situ FTIR

3.7.1. In situ FTIR of the activation of reactants

In situ FTIR experiments have been conducted over Ce-Ti and Co-Ce-Ti samples to investigate the formation and transformation of surface adsorbed species, which provide the important information for clarifying the activation capacity of the catalysts, the reaction pathway of intermediates, and the reaction mechanism.

Fig. 8 shows the FTIR spectra of surface adsorbed species deriving from the co-adsorption of NO and O₂ at different temperatures over Ce-Ti and Co-Ce-Ti samples. For Ce-Ti sample, *in situ* contact of NO and O₂ at room temperature resulted in the detection of the bands centered at 1628 and 1468 cm⁻¹, corresponding to the asymmetric stretching of coordinatively held NO₂ formed by NO oxidation and the M-NO₂ (M = Co, Ce or Ti) nitro compounds, respectively [39,50]. With the increase of temperature, the main surface adsorbed species transformed to nitrates with different configurations, including bridging nitrates (1605 and 1245–1235 cm⁻¹), bidentate nitrate (1580 and 1541 cm⁻¹) and the free nitrate ions (1359 cm⁻¹) [9,51,52]. For Co-Ce-Ti sample, the nitrates species, including bridging nitrates (1604 and 1251 cm⁻¹), bidentate nitrates (1580 and 1520 cm⁻¹) and monodentate nitrates (1295 cm⁻¹) [19,53], were produced at room temperature, co-existing with NO₂ and M-NO₂ (1633 and 1467 cm⁻¹). The change of the spectra with the reaction temperatures over Co-Ce-Ti sample was similar to that over Ce-Ti sample. Fig. 8b and d illustrated that more adsorbed NO_x species were generated over Co-Ce-Ti sample than that over Ce-Ti sample, and the formation of nitrates species occurred at room temperature, suggesting the enhancement of NO

activation. The improvement of the capacity towards NO activation over Co-Ce-Ti sample could be attributed to the abundant surface adsorbed oxygen, induced by the aggravation of lattice distortion of Ce–O–Co bond with strong interaction.

The FTIR spectra of NH₃ adsorption over Ce-Ti and Co-Ce-Ti samples at different reaction temperatures are presented in Fig. 9. For Ce-Ti sample, the NH₃ adsorption at room temperature led to the appearance of the bands attributed to NH₃ bound to Lewis acid sites (1597, 1300, 1189 and 1163 cm⁻¹) and ionic NH₄⁺ bound to Brønsted acid sites (1665, 1465 and 1435 cm⁻¹) [50,54,55], which were denoted as NH₃(L) and NH₄⁺(B), respectively. The band around 1108 cm⁻¹ was ascribed to the hydrogen–nitrogen bonds, and the bands centered at 1580 and 1065 cm⁻¹ were assigned to the bond between the hydrogen atom from NH₃ and the surface oxygen atom [50,56]. In the high wavenumber range, the bands around 3343, 3250 and 3157 cm⁻¹ were referred to NH₃(L) [57], and the band at 3395 cm⁻¹ was attributed to NH₂ groups [58]. The bands around 3734 and 3675 cm⁻¹ were attributed to the vibrations of –OH bound to the surface metal atoms [58]. With the increase of temperature, a new band with weak intensity appeared at 1521 cm⁻¹, associated to split ν_3 mode of bidentate nitrates and indicating the oxidation of NH₃ by surface oxygen [53]. Meanwhile, the enhancement of the intensity of the band around 1580 cm⁻¹ also suggested the effective activation of NH₃. For the Co-Ce-Ti sample, a new band was detected at 1227 cm⁻¹, which was also attributed to NH₃(L) and suggested the production of extra Lewis acid sites induced by the introduction of Co [59]. The negative band around 3628 cm⁻¹ was assigned to the Brønsted OH groups caused by the adsorption of NH₄⁺ at Brønsted acid [58]. Moreover, compared with Ce-Ti sample, the band suggesting the interaction between NH₃ and surface oxygen (1575 cm⁻¹) on Co-Ce-Ti sample appeared at a lower temperature of 140 °C, herein it was considered that the incorporation of Co enhanced the capacity of catalyst towards NH₃ activation.

To further clarify the effect of Co-doping on the types and quantities of adsorbed species, the areas of the characteristic peaks, assigned to various species during NO + O₂ co-adsorption and NH₃ adsorption at 25 and 140 °C in Figs. 8 and 9, have been integrated (Fig. 10). From Fig. 10a, it was apparent that more adsorbed NO₂, M-NO₂, and nitrates species were generated over Co-Ce-Ti sample at room temperature, suggesting the much stronger capacity of Co-Ce-Ti sample towards NO activation. The improvement in the generation of adsorbed NO₂ quite favored the low-temperature activity via the “fast-SCR”, and also benefited the production of nitrate species, which were considered as the main intermediates for the generation of N₂ at high temperatures. Fig. 10b compares the quantities of Lewis and Brønsted acid sites over Ce-Ti and Co-Ce-Ti samples, illustrating that the introduction of Co increased the quantity and percentage of Lewis acid sites on the catalyst surface. The results of *in situ* FTIR of NH₃ adsorption were well agreement with the information derived from NH₃-TPD, also confirmed the speculation that the primary surface acid was Lewis acid and the Co-doping facilitated the formation of Lewis acid sites, as referred in Section 3.6. According to previous reports [19,49], the Lewis acid sites are produced by the coordinatively unsaturated cationic sites, and therefore are readily to act as electron acceptors to react with NO molecules directly, which possessed the one-electron bond in electronic structure. And the Lewis acid sites could also activate the oxygen by electrostatic polarization, attacked by gas-phase NO to form NO₂ [60]. Herein, the more surface Lewis acid sites, the more adsorption and activation sites for NO, which could be crucial for the promotion of the generation of adsorbed NO₂ and nitrates species on Co-Ce-Ti, as well as the elevated catalytic activity.

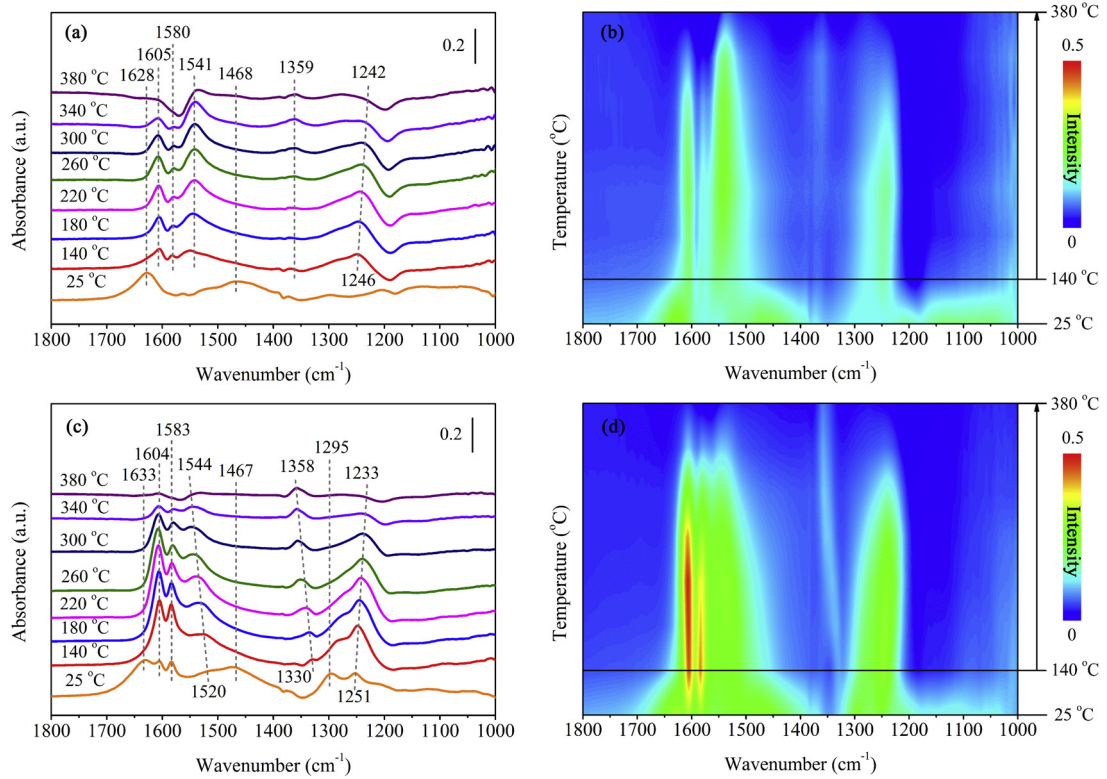


Fig. 8. *In situ* FTIR spectra of surface species deriving from NO and O₂ co-adsorption over Ce-Ti (a and b) and Co-Ce-Ti (c and d) samples at different temperatures. Conditions: [NO] = 500 ppm, [O₂] = 5 vol.%, and He as balance.

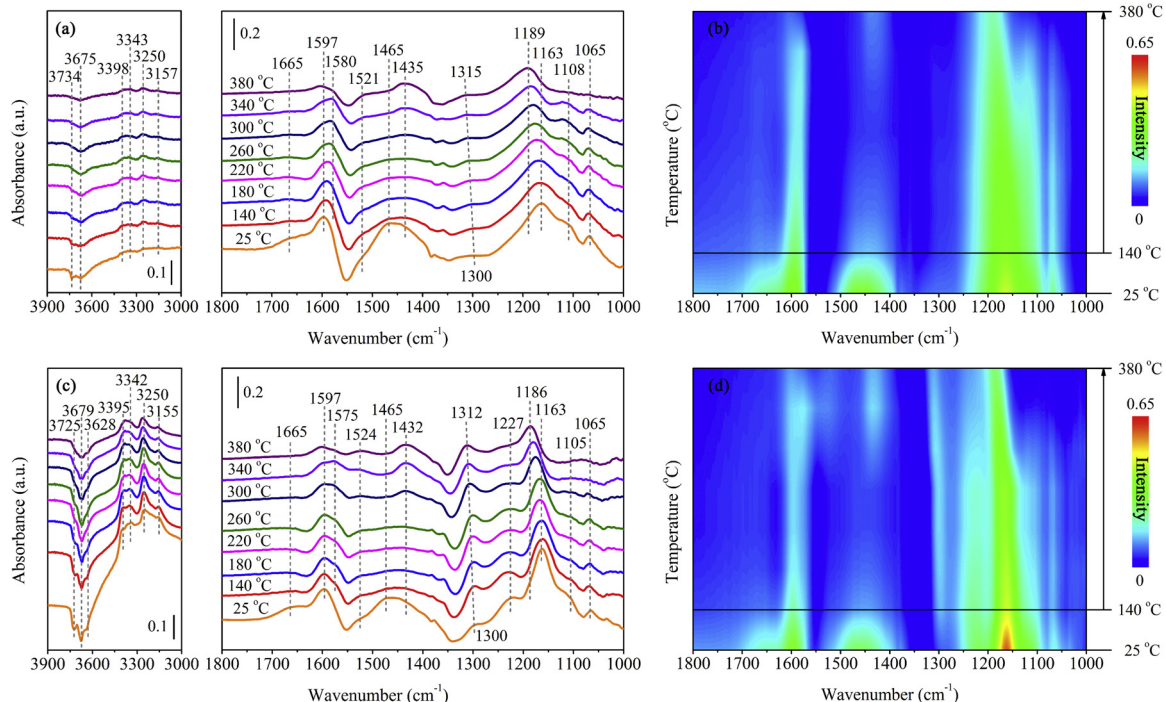


Fig. 9. *In situ* FTIR spectra of NH₃ adsorption depending on reaction temperatures over Ce-Ti (a) and Co-Ce-Ti (b) samples. Conditions: [NH₃] = 500 ppm, and He as balance.

3.7.2. Reaction of NH₃ with pre-adsorbed NO + O₂

Transient FTIR experiments were also carried out to clarify the reaction mechanism of N₂ generation over Ce-Ti and Co-Ce-Ti catalysts. *In situ* FTIR spectra of the reaction between NH₃ and pre-adsorbed NO_x species deriving from NO + O₂ co-

adsorption are displayed in Fig. 11. For Ce-Ti catalyst, the NO + O₂ co-adsorption and He purging resulted in the appearance of bridging nitrates (1604 and 1245 cm⁻¹) and bidentate nitrates (1579 and 1558 cm⁻¹), and the shoulder band with weak intensity around 1293 cm⁻¹ was attributed to the monodentate nitrates. After the

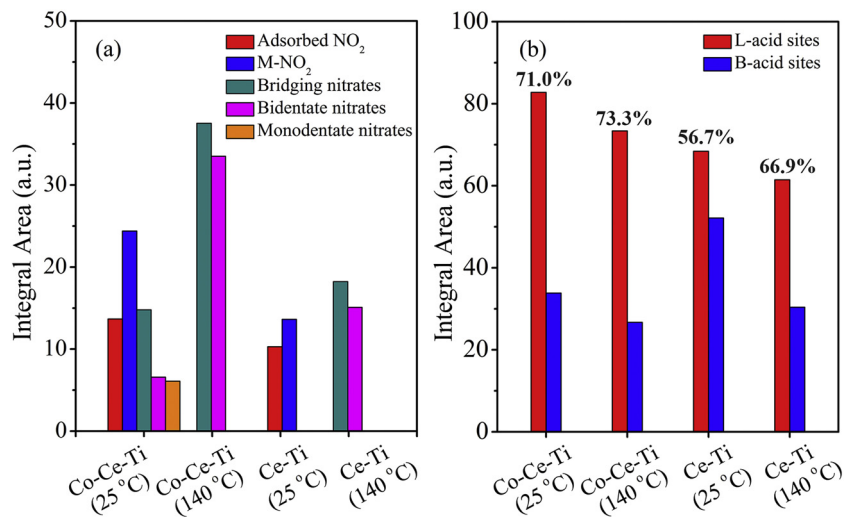


Fig. 10. Relative quantities of various adsorbed NO_x species derived from $\text{NO} + \text{O}_2$ co-adsorption (a) and Lewis acid sites and Brønsted acid sites calculated by NH_3 adsorption (b).

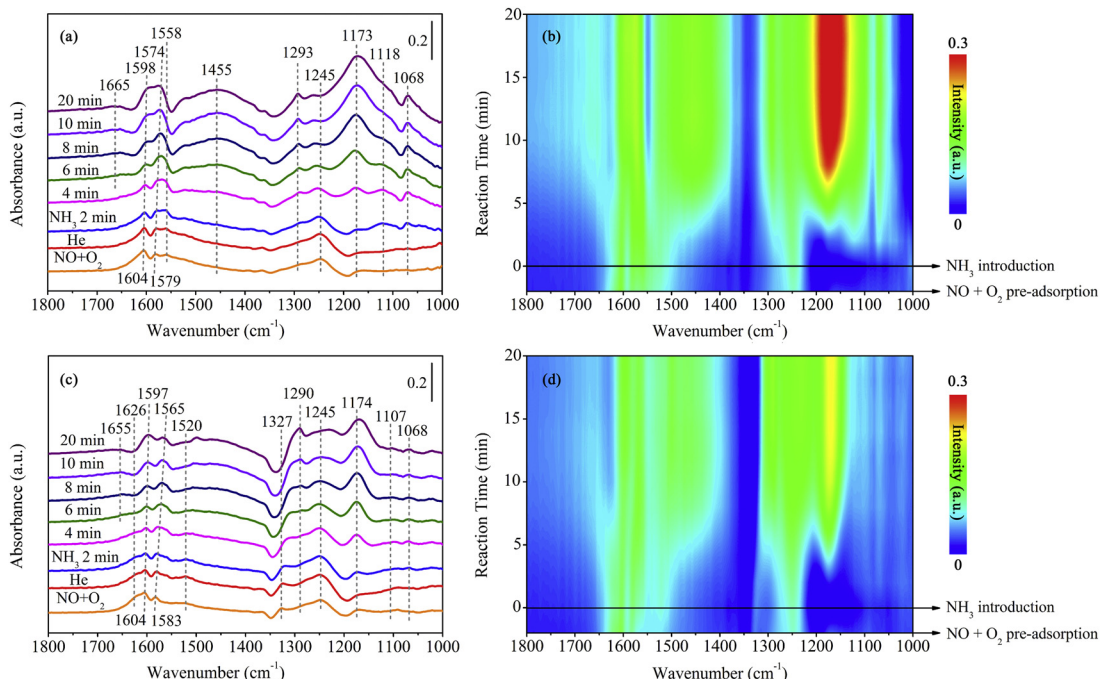


Fig. 11. *In situ* FTIR spectra of NH_3 reacted with pre-adsorbed NO_x species over Ce-Ti (a and b) and Co-Ce-Ti (c and d) samples at 140°C . Conditions: $[\text{NO}] = 500 \text{ ppm}$ (when used), $[\text{NH}_3] = 500 \text{ ppm}$ (when used), $[\text{O}_2] = 5 \text{ vol.\%}$ (when used), and He as balance.

introduction of NH_3 , the intensity of the bands around 1604 and 1579 cm^{-1} decreased gradually, and shifted to the lower wavenumbers of 1598 and 1574 cm^{-1} , respectively. Meanwhile, the intensity of the bands around 1558 and 1245 cm^{-1} was also decreased gradually with the reaction time and disappeared totally. Both the blue shift of the wavenumber and the decrease of the intensity suggested the consumption of surface nitrate species. Then the catalyst surface was mainly covered by the adsorbed NH_3 species, including $\text{NH}_3(\text{L})$ (1598 , 1293 and 1173 cm^{-1}) and $\text{NH}_4^+(\text{B})$ species (1665 and 1455 cm^{-1}). The appearance of the bands around 1574 , 1118 and 1068 cm^{-1} also indicated the adsorption and oxidation of NH_3 . The changes of the spectra over Ce-Ti sample illustrated the efficient reaction between NH_3 and pre-adsorbed NO_x species, according with the Langmuir-Hinshelwood (L-H) mechanism of NH_3 -SCR reaction.

For Co-Ce-Ti sample, bridging (1604 and 1245 cm^{-1}), bidentate (1583 and 1520 cm^{-1}) and monodentate nitrates (1290 cm^{-1}) were also formed after the pre-adsorption of $\text{NO} + \text{O}_2$, meanwhile adsorbed NO_2 (1626 cm^{-1}) and free nitrate ions (1330 cm^{-1}) also appeared. The L-H mechanism also suggested on Co-Ce-Ti sample as the characteristic bands of the adsorbed NO_x species exhibited a significant decrease in intensity or a blue shift of the wavenumber after the introduction of NH_3 . Moreover, the presence of adsorbed NO_2 on Co-Ce-Ti sample further favored the low-temperature activity by "fast SCR". Comparing the results presented in Fig. 11b and d, it was noted that the intensity of the bands around 1580 and 1065 cm^{-1} over Co-Ce-Ti sample was much weaker than that over Ce-Ti sample, whereas they exhibited the similar intensities over the two samples in the experiment of NH_3 adsorption (Fig. 9). The above two bands reflected the interaction between H atom from

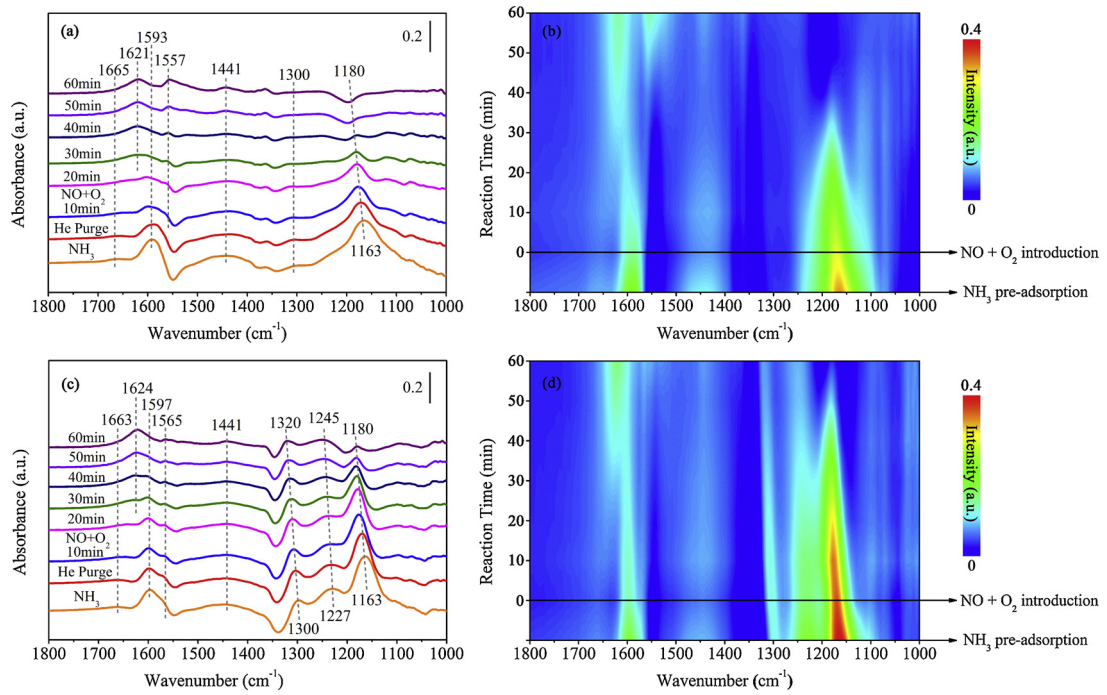
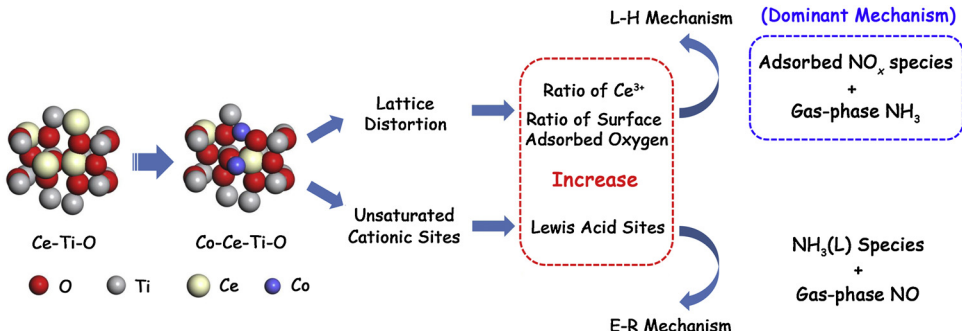


Fig. 12. *In situ* FTIR spectra of NO + O₂ reacted with pre-adsorbed NH₃ species over Ce-Ti (a and b) and Co-Ce-Ti (c and d) samples at 140 °C. Conditions: [NO] = 500 ppm (when used), [NH₃] = 500 ppm (when used), [O₂] = 5 vol.% (when used), and He as balance.



Scheme 1. The proposed NH₃-SCR reaction mechanism over Co-Ce-Ti sample.

NH₃ with a surface oxygen atom, herein, it was illustrated that the oxidation of NH₃ facilitated by the adsorbed NO_x over Co-Ce-Ti sample was not as obvious as that over Ce-Ti sample, which also suggested the possible inhibition of the combustion of NH₃ caused by the incorporation of Co.

3.7.3. Reaction of NO + O₂ with pre-adsorbed NH₃

To compare the reactivity of the adsorbed NH₃ species in SCR reaction over Ce-Ti and Co-Ce-Ti catalysts, *in situ* FTIR spectra of the reaction between NO + O₂ and pre-adsorbed NH₃ were recorded (Fig. 12). As presented in Fig. 12a, Ce-Ti catalyst was firstly saturated by the adsorbed NH₃ species, including NH₃(L) (1593, 1300 and 1163 cm⁻¹) and NH₄⁺(B) species (1665 and 1441 cm⁻¹). After the introduction of NO + O₂, the NH₃(L) species (1569, 1300 and 1163 cm⁻¹) exhibited a rapid consumption, but the consumption not happened for NH₄⁺(B) species (1441 cm⁻¹). The much quicker consumption of NH₃(L) species compared with that of NH₄⁺(B) species, which could be observed clearly in Fig. 12b, illustrated the role of NH₃(L) as the main active intermediates, and its reaction with gas-phase NO suggested the presence of Eley-Rideal (E-R) mechanism. After that the excess introduction of NO + O₂ resulted in the formation and accumulation of nitrates species on the cat-

alyst surface, leading to the appearance of the bridging nitrates (1621 cm⁻¹) and bidentate nitrates (1557 cm⁻¹).

For Co-Ce-Ti catalyst, the NH₃(L) and NH₄⁺(B) species were also generated by the pre-adsorption of NH₃ and further reacted with gas-phase NO, similar to that over Ce-Ti sample and suggested the E-R mechanism. In Fig. 12c, the new band appearing around 1227 cm⁻¹ was also assigned to NH₃(L) species. Comparing the results presented in Fig. 12b and d, Co-Ce-Ti sample exhibited the much higher capacity towards NH₃ activation, and greatly promoted the generation of NH₃(L) species (1597, 1300 and 1163 cm⁻¹), which were considered as the initial intermediates in E-R mechanism. As discussed in Section 3.7.1, more Lewis acid sites were induced over Co-Ce-Ti sample due to the coordinatively unsaturated cationic sites caused by the partial substitution of Ce by Co atoms, and the further promoted generation of NH₃(L) species was considered to elevate the low-temperature activity. Moreover, a new shoulder band appeared at 1565 cm⁻¹ and was assigned to the amide species (–NH₂) formed by the dehydrogenation of the adsorbed NH₃ [61]. The –NH₂ species has been reported as a precursor for the intermediate of NH₂NO, which is generated by the direct reaction between –NH₂ and gas-phase or weakly adsorbed NO, and further decomposes to N₂ and H₂O [39,57,61]. Due to the

easy overlap of the characteristic bands of $-\text{NH}_2$ and bidentate nitrates, the appearance of $-\text{NH}_2$ means a possible new pathway for the formation of N_2 over Co-Ce-Ti sample.

Compared with the reaction between NH_3 and the adsorbed NO_x species, which completed in about 8 min (Fig. 11), the reaction between NO and the adsorbed NH_3 was much slower, suggesting that the L-H mechanism could be the dominant reaction pathway for the generation of N_2 over Ce-Ti and Co-Ce-Ti samples. This phenomenon is in agreement with previous reports about Ce-containing catalysts [27,62,63], attributing to the higher energy barrier of the first step of the E-R mechanism compared with that of L-H mechanism, which has been further confirmed by density functional theory calculation [64].

3.7.4. Proposed reaction mechanism

Based on the physico-chemical characterizations and *in situ* FTIR, the mechanism for the improvement of the low-temperature activity of Co-Ce-Ti sample was proposed, which was displayed in Scheme 1 and described as follows.

- (i) Both the L-H and E-R mechanisms occurred during the NH_3 -SCR reaction, and the L-H mechanism was the dominant process due to its lower reaction barrier.
- (ii) For the L-H mechanism, the introduction of Co increased the ratio of surface Ce^{3+} and adsorbed oxygen species by aggravating the lattice distortion, and favored the adsorption and activation of NO molecules, especially benefited the formation of adsorbed NO_2 . Then the reaction between the adsorbed NO_x species and gas-phase NH_3 was promoted, and the low-temperature activity could be further elevated by the “fast SCR” reaction. Besides, the oxidation of NH_3 over Co-Ce-Ti sample was also inhibited, which could be accelerated greatly by the surface adsorbed NO_x species and served as the main side reaction of SCR reaction.
- (iii) For the E-R mechanism, $\text{NH}_3(\text{L})$ species were considered as the most important initial intermediates. Owing to the coordinatively unsaturated cationic sites caused by the partial substitution of Ce by Co, more Lewis acid sites were produced on Co-Ce-Ti sample and therefore promoted the generation of $\text{NH}_3(\text{L})$ species. On the other hand, $-\text{NH}_2$ species were speculated to generate on Co-Ce-Ti sample, and the further decomposition of $-\text{NH}_2$ species could be an additional pathway for the production of N_2 .

4. Conclusions

A series of Ce-Ti mixed oxides decorated by transition metals with variable valence (Co, Cu and Fe) were synthesized to enhance the low-temperature activity of NH_3 -SCR reaction. Among the as-prepared samples, Co-Ce-Ti demonstrated remarkable deNO_x performance with elevated low-temperature activity and broadened temperature window. The quite different atom size of Co from Ce, the strong interaction of the Co–O–Ce bond and the variable valence of Co enhanced the lattice distortion of Ce-Ti mixed oxide, and consequently improved the ratio of surface Ce^{3+} species as well as the quantity of oxygen vacancies, benefiting the adsorption and activation of reactants. During the NH_3 -SCR reaction, both the L-H and E-R mechanisms were present over the Co-Ce-Ti sample. The higher ratio of surface Ce^{3+} and adsorbed oxygen species over Co-Ce-Ti sample promoted the adsorption and activation of NO , and facilitated the reaction between the adsorbed NO_x species and the gas-phase NH_3 , which followed the L-H mechanism. For the E-R mechanism, $\text{NH}_3(\text{L})$ species were illustrated to be the crucial initial intermediates for NH_3 activation, and the more Lewis acid sites on Co-Ce-Ti sample, which were attributed to its coordinatively unsat-

urated cationic sites, benefited the reaction between the adsorbed NH_3 species and NO molecules. Due to the rapid reaction rate, the L-H mechanism was considered as the dominate one during the NH_3 -SCR reaction at low temperatures, and the improvements in both of the L-H and E-R reactions contributed the elevated low-temperature activity of Co-Ce-Ti sample.

Acknowledgements

This work was supported financially by the National Nature Science Foundation of China (21507029, 21501138), Nature Science Foundation of Hebei Province (B2016502063), Open Foundation of Key Laboratory of Industrial Ecology and Environmental Engineering (KLIEE-15-02), China Ministry of Education and the Fundamental Research Funds for the Central Universities (2016MS109, 2015ZD25), and Australian Research Council (DP150103026).

Appendix A. Supplementary data

Supplementary data associated with this article can be found, in the online version, at <http://dx.doi.org/10.1016/j.apcatb.2016.07.020>.

References

- [1] D.K. Pappas, T. Boningari, P. Boolchand, P.G. Smirniotis, *J. Catal.* 334 (2016) 1–13.
- [2] X. Xiao, S. Xiong, Y. Shi, W. Shan, S. Yang, *J. Phys. Chem. C* 120 (2016) 1066–1076.
- [3] D. Meng, W. Zhan, Y. Guo, Y. Guo, L. Wang, G. Lu, *ACS Catal.* 5 (2015) 5973–5983.
- [4] P. Sudarsanam, B. Hillary, B. Mallesham, B.G. Rao, M.H. Amin, A. Nafady, A.M. Alsalmi, B.M. Reddy, S.K. Bhargava, *Langmuir* 32 (2016) 2208–2215.
- [5] W. Yao, Y. Liu, X. Wang, X. Weng, H. Wang, Z. Wu, *J. Phys. Chem. C* 120 (2016) 221–229.
- [6] G. Chen, Q. Xu, Y. Yang, C. Li, T. Huang, G. Sun, S. Zhang, D. Ma, X. Li, *ACS Appl. Mater. Interfaces* 7 (2015) 23538–23544.
- [7] H. Chang, Q. Wu, T. Zhang, M. Li, X. Sun, J. Li, L. Duan, J. Hao, *Environ. Sci. Technol.* 49 (2015) 12388–12394.
- [8] P. Li, Y. Xin, Q. Li, Z. Wang, Z. Zhang, L. Zheng, *Environ. Sci. Technol.* 46 (2012) 9600–9605.
- [9] L. Zhang, L. Li, Y. Cao, X. Yao, C. Ge, F. Gao, Y. Deng, C. Tang, L. Dong, *Appl. Catal. B: Environ.* 165 (2015) 589–598.
- [10] Y. Liu, W. Yao, X. Cao, X. Weng, Y. Wang, H. Wang, Z. Wu, *Appl. Catal. B: Environ.* 160–161 (2014) 684–691.
- [11] Z. Liu, S. Zhang, J. Li, L. Ma, *Appl. Catal. B: Environ.* 144 (2014) 90–95.
- [12] S. Cai, D. Zhang, L. Zhang, L. Huang, H. Li, R. Gao, L. Shi, J. Zhang, *Catal. Sci. Technol.* 4 (2014) 93–101.
- [13] X. Wang, W. Wen, Y. Su, R. Wang, *RSC Adv.* 5 (2015) 63135–63141.
- [14] Y. Li, Y. Wan, Y. Li, S. Zhan, Q. Guan, Y. Tian, *ACS Appl. Mater. Interfaces* 8 (2016) 5224–5233.
- [15] J. Han, J. Meeprasert, P. Maitarad, S. Nammuangruk, L. Shi, D. Zhang, *J. Phys. Chem. C* 120 (2016) 1523–1533.
- [16] H. Hu, S. Cai, H. Li, L. Huang, L. Shi, D. Zhang, *ACS Catal.* 5 (2015) 6069–6077.
- [17] F. Zhao, Z. Liu, W. Xu, S. Yao, A. Kubacka, A.C. Johnston-Peck, S.D. Senanayake, A.-Q. Zhang, E.A. Stach, M. Fernández-García, J.A. Rodriguez, *J. Phys. Chem. C* 118 (2014) 2528–2538.
- [18] X. Wang, W. Wen, J. Mi, X. Li, R. Wang, *Appl. Catal. B: Environ.* 176–177 (2015) 454–463.
- [19] Z. Liu, Y. Yi, J. Li, S.I. Woo, B. Wang, X. Cao, Z. Li, *Chem. Commun.* 49 (2013) 7726–7728.
- [20] K.A. Michalow-Mauke, Y. Lu, K. Kowalski, T. Graule, M. Nachtegaal, O. Kröcher, D. Ferri, *ACS Catal.* 5 (2015) 5657–5672.
- [21] L. Qiu, D. Pang, C. Zhang, J. Meng, R. Zhu, F. Ouyang, *Appl. Surf. Sci.* 357 (2015) 189–196.
- [22] T. Boningari, P.R. Ettireddy, A. Somogyvari, Y. Liu, A. Vorontsov, C.A. McDonald, P.G. Smirniotis, *J. Catal.* 325 (2015) 145–155.
- [23] Y. Liu, J. Xu, H. Li, S. Cai, H. Hu, C. Fang, L. Shi, D. Zhang, *J. Mater. Chem. A* 3 (2015) 11543–11553.
- [24] L. Zhang, L. Shi, L. Huang, J. Zhang, R. Gao, D. Zhang, *ACS Catal.* 4 (2014) 1753–1763.
- [25] H. Hu, S. Cai, H. Li, L. Huang, L. Shi, D. Zhang, *J. Phys. Chem. C* 119 (2015) 22924–22933.
- [26] G. Busca, L. Lietti, G. Ramis, F. Berti, *Appl. Catal. B: Environ.* 18 (1998) 1–36.
- [27] Y. Peng, K. Li, J. Li, *Appl. Catal. B: Environ.* 140–141 (2013) 483–492.
- [28] Hui Wang, Zhenping Qu, Hongbin Xie, Nobutaka Maeda, Lei Miao, Zhong Wang, *J. Catal.* 338 (2016) 56–67.

[29] S. Wang, L. Pan, J.J. Song, W. Mi, J.J. Zou, L. Wang, X. Zhang, *J. Am. Chem. Soc.* 137 (2015) 2975–2983.

[30] C. Canevali, M. Mattoni, F. Morazzoni, R. Scotti, M. Casu, A. Musinu, R. Krsmanovic, S. Polizzi, A. Speghini, M. Bettinelli, *J. Am. Chem. Soc.* 127 (2005) 14681–14691.

[31] A. Martínez-Arias, M. Fernández-García, A.B. Hungría, J.C. Conesa, G. Munuera, *J. Phys. Chem. B* 107 (2003) 2667–2677.

[32] M. Martínezhuerta, *J. Catal.* 225 (2004) 240–248.

[33] I. Moog, C. Feral-Martin, M. Duttine, A. Wattiaux, C. Prestipino, S. Figueiroa, J. Majimel, A. Demourgues, *J. Mater. Chem. A* 2 (2014) 20402–20414.

[34] G. Li, R.L. Smith Jr., H. Inomata, *J. Am. Chem. Soc.* 123 (2001) 11091–11092.

[35] A.B. Hungría, A. Martínez-Arias, M. Fernández-García, A. Iglesias-Juez, A. Guerrero-Ruiz, J.J. Calvino, J.C. Conesa, J. Soria, *Chem. Mater.* 15 (2003) 4309–4316.

[36] P. Burroughs, A. Hamnett, A.F. Orchard, G. Thornton, *J. Chem. Soc. Dalton Trans.* 17 (1976) 1686–1698.

[37] F. Zhang, S. Zhang, N. Guan, E. Schreier, M. Richter, R. Eckelt, R. Fricke, *Appl. Catal. B: Environ.* 73 (2007) 209–219.

[38] L. Óvári, S. Krick Calderon, Y. Lykhach, J. Libuda, A. Erdőhelyi, C. Papp, J. Kiss, H.P. Steinrück, *J. Catal.* 307 (2013) 132–139.

[39] F. Yan, Y. Wang, J. Zhang, Z. Lin, J. Zheng, F. Huang, *ChemSusChem* 7 (2014) 101–104.

[40] B. Meng, Z. Zhao, X. Wang, J. Liang, J. Qiu, *Appl. Catal. B: Environ.* 129 (2013) 491–500.

[41] F. Bin, C. Song, G. Lv, J. Song, X. Cao, H. Pang, K. Wang, *J. Phys. Chem. C* 116 (2012) 26262–26274.

[42] F. Liu, H. He, C. Zhang, Z. Feng, L. Zheng, Y. Xie, T. Hu, *Appl. Catal. B: Environ.* 96 (2010) 408–420.

[43] Z. Wang, Z. Qu, X. Quan, Z. Li, H. Wang, R. Fan, *Appl. Catal. B: Environ.* 134–135 (2013) 153–166.

[44] T. Bao, Z. Zhao, Y. Dai, X. Lin, R. Jin, G. Wang, T. Muhammad, *Appl. Catal. B: Environ.* 119–120 (2012) 62–73.

[45] F.L.S. Carvalho, Y.J.O. Asencios, A.M.B. Rego, E.M. Assaf, *Appl. Catal. A: Gen.* 483 (2014) 52–62.

[46] S.N.R. Inturi, T. Boningari, M. Suidanb, P.G. Smirniotis, *Appl. Catal. B: Environ.* 144 (2014) 333–342.

[47] L. Xue, C. Zhang, H. He, Y. Teraoka, *Catal. Today* 126 (2007) 449–455.

[48] D. Yuan, X. Li, Q. Zhao, J. Zhao, M. Tadé, S. Liu, *J. Catal.* 309 (2014) 268–279.

[49] D. Yuan, X. Li, Q. Zhao, J. Zhao, S. Liu, M. Tadé, *Appl. Catal. A: Gen.* 451 (2013) 176–183.

[50] M. Casapu, O. Kröcher, M. Mehring, M. Nachtegaal, C. Borca, M. Harfouche, D. Grolimund, *J. Phys. Chem. C* 114 (2010) 9791–9801.

[51] H. Wang, L. Zhang, Z. Chen, J. Hu, S. Li, Z. Wang, J. Liu, X. Wang, *Chem. Soc. Rev.* 43 (2014) 5234–5244.

[52] R. Jin, Y. Liu, Y. Wang, W. Cen, Z. Wu, H. Wang, X. Weng, *Appl. Catal. B: Environ.* 148–149 (2014) 582–588.

[53] P.R. Ettireddy, N. Ettireddy, T. Boningari, R. Pardemann, P.G. Smirniotis, *J. Catal.* 292 (2012) 53–63.

[54] S. Yang, S. Xiong, Y. Liao, X. Xiao, F. Qi, Y. Peng, Y. Fu, W. Shan, J. Li, *Environ. Sci. Technol.* 48 (2014) 10354–10362.

[55] F. Giraud, C. Geantet, N. Guilhaume, S. Gros, L. Porcheron, M. Kanniche, D. Bianchi, *J. Phys. Chem. C* 118 (2014) 15664–15676.

[56] W. Chen, Y. Ma, Z. Qu, Q. Liu, W. Huang, X. Hu, N. Yan, *Environ. Sci. Technol.* 48 (2014) 12199–12205.

[57] F. Liu, W. Shan, Z. Lian, L. Xie, W. Yang, H. He, *Catal. Sci. Technol.* 3 (2013) 2699–2707.

[58] L. Wang, W. Li, S.J. Schmieg, D. Weng, *J. Catal.* 324 (2015) 98–106.

[59] B. Thirupathi, P.G. Smirniotis, *J. Catal.* 288 (2012) 74–83.

[60] E. Kikuchi, K. Yogo, *Catal. Today* 22 (1994) 73–86.

[61] D. Sun, Q. Liu, Z. Liu, G. Gui, Z. Huang, *Appl. Catal. B: Environ.* 92 (2009) 462–467.

[62] L. Zhang, J. Pierce, V.L. Leung, D. Wang, W.S. Epling, *J. Phys. Chem. C* 117 (2013) 8282–8289.

[63] Y. Peng, C. Wang, J. Li, *Appl. Catal. B: Environ.* 144 (2014) 538–546.

[64] B. Liu, J. Liu, S. Ma, Z. Zhao, Y. Chen, X.Q. Gong, W. Song, A. Duan, G. Jiang, *J. Phys. Chem. C* 120 (2016) 2271–2283.